Copy No. _____

Defence Research and Development Canada
Recherche et développement pour la défense Canada

DEFENCE R&D DÉFENSE

Validations of Computational Weld Models

Comparison of Residual Stresses

John Goldak

Prepared by:
Goldak Technology Inc.
3745 Revelstoke Drive
Ottawa, Ontario K1V 7C2

Project Manager: John Porter, 902-427-3423
Contract Number: W7707-098193
Contract Scientific Authority: Christopher Bayley, 205-363-4784

Defence R&D Canada – Atlantic

Contract Report
DRDC Atlantic CR 2009-222
August 2010

Canada

This page intentionally left blank.

Validations of Computational Weld Models

Comparison of Residual Stresses

John Goldak

Prepared by:

Goldak Technology Inc.
3745 Revelstoke Drive, Ottawa, ON, K1V7C2, Canada

Project Manager: John Porter (902) 427 3423
Contract Number: W7707-098193
Contract Scientific Authority: Christopher Bayley (250) 363-4784

Defence R&D Canada – Atlantic

Contract Report

DRDC Atlantic CR 2009-222

August 2010

Principal Author

Original signed by John Goldak

John Goldak

Approved by

Original signed by Dr. T. Foster

Dr .T. Foster
Head/DLP

Approved for release by

Original signed by Ron Kuwahara for

Dr. C. Hyatt
Head/Document Review Panel

Abstract

The objective of this project was to validate the capability of *VrWeld* to simulate the weld build-up process in two experimental setups. Setup I had a central depression with dimensions of $100 \times 100 \times 3$ mm, while Setup II had a central depression with dimensions of $200 \times 200 \times 3$ mm.

This report documents the validation of the computer model's capability to compute residual stress in overlay weld repairs of this type, i.e., does the model predict the measured residual stress with sufficient accuracy, reliability and robustness.

For this project, the values of the computed residual stress data were mapped to the data points at which the residual stress was measured. Then two types of plots were made. The first is an image of the stress field determined by linear interpolation onto the prefered grid. The second is a plot of curves of the computed residual stress data and the residual stress along lines in the plane of the panel. For both types, one image of measured and one image of computed data is shown on each page to facilitate comparison.

Whether the model predicts the measured residual stress with sufficient accuracy, reliability and robustness for a particular analysis would depend on the analysis.

Résumé

Le projet qui fait l'objet du présent rapport a comme objectif de valider la capacité du logiciel *VrWeld* de simuler le procédé de soudage de rechargement de deux montages expérimentaux. Le montage I présente une dépression centrale mesurant 100 mm sur 100 mm sur 3 mm, tandis que le montage II en présente une dont les dimensions sont de 200 mm sur 200 mm sur 3 mm.

Le présent rapport traite des travaux visant à valider la capacité du modèle informatique de calculer les contraintes résiduelles dans des structures réparées par ce type de soudage de rechargement ; en d'autres mots, il s'agit d'établir si les prévisions du modèle, en matière de contraintes résiduelles mesurées, sont adéquates au chapitre de l'exactitude, de la fiabilité et de la robustesse.

Dans le cadre du présent projet, on a réalisé la mise en correspondance des valeurs calculées de contraintes résiduelles et des points de données où les contraintes résiduelles ont été effectivement mesurées. Par la suite, deux types de graphiques ont été tracés. Ceux du premier type constituent une image du champ de contraintes déterminé par interpolation linéaire sur le maillage privilégié. Ceux du second type constituent un tracé des courbes des valeurs calculées de contraintes résiduelles, le long de lignes se trouvant dans le plan du panneau. Dans les deux cas, afin de faciliter la comparaison, chaque page comprend une

image des valeurs mesurées et une autre des valeurs calculées.

Le processus visant à déterminer si le modèle permet ou non de prévoir les contraintes résiduelles mesurées avec des degrés adéquats d'exactitude, de fiabilité et de robustesse, est fonction de l'analyse réalisée.

Executive summary

Validations of Computational Weld Models: Comparison of Residual Stresses

John Goldak; DRDC Atlantic CR 2009-222; Defence R&D Canada – Atlantic; August 2010.

Background: When welding is used to to repair damage caused by corrosion, accidents, or re-sealing interior accesses to the pressure hull of a submarine, changes in the geometry, residual stresses and material properties have the potential to affect its in-service behaviour. In particular, there is a need to develop the capability to estimate the extent to which welding changes the resistance of the pressure hull to buckling, fatigue and fracture.

To this end, DRDC Atlantic commissioned BMT Fleet Technologies Limited to make overlay welds on two rigid panels. The structures were instrumented with thermocouples and strain gauges which recorded the change in temperature and strains during the preheating, welding, and cool-down. The distortion of the bottom of the plate in the final structure was measured and reported in *Monitoring of Welding Induced Strains during Cladding* [1].

DRDC Atlantic commissioned Goldak Technologies Inc. to model the overlay welding procedure used to make the two panels to predict the transient distortion, strain and stress in the two rigid panels. These results are summarized in the report *Thermo-mechanical modelling of welding induced strains: Numerical validation of the weld build-up process* [2].

This document reports on the comparison of residual stresses in the two panels measured by neutron diffraction and computed by the computational weld mechanics software *VrWeld*.

Principal results:

1. The 100×100 mm built-up region were simulated using 27 overlay weld passes while the 200×200 mm built-up region was simulated with 51 overlay weld passes.

2. The influence of filler metal chemistry was also included for two cases.

3. The residual stresses in experimental setup I with the 100×100 mm built-up region and experimental setup II with the 200×200 mm built-up region computed by a computational weld mechanics model,*VrWeld*, and measured by neutron diffraction were compared. In the experimetal setup the resiidual stresses were were measured at points in the longitudinal and transverse planes.

4. While a visual examination of the residual stress plots suggest that there is some agreement between the measured and computed values of residual stress, to the author's knowledge, no generally accepted methods to compute a quantitative measure of the agreement are available.

Significance of results: To validate the computer model, an application must be defined and the sensitivity of the model results to that application must be determined. Whether this agreement is sufficient for a particular design decision would depend on the applications.

Future work: Based on past and current experience, the following recommendation and future work are suggested:

A virtual Design of Experiment (DOE) should be done to determine the sensitivity of the solution to model parameters. This would enable the agreement between measured and computed residual stress to be improved. The computed longitudinal stresses in the weld metal appear to be higher than the measured longitudinal stresses. This higher tensile residual stress in the weld metal could generate the higher longitudinal compressive stress just below the high tensile stress. This suggests that it would be worth doing a DOE analysis to compute the sensitivity to changes in the yield stress of martensite and bainite phases to determine if this improves the agreement between measured and computed residual stress.

The effect of martensite on the tempering to reduce the hardness of martensite formed in one weld pass by a later pass should be analyzed. This reduction in hardness suggests that the yield stress of martensite be reduced from approximately 900 MPa of the untempered martensite. If a model is developed for tempering of martensite, then the model could be included in the computer model.

Hardness measurements of the plate suggest that the hardness has a significant fluctuations in space, i.e., it is not homogeneous. It would be of interest to study the effect of such fluctuations on the residual stress. Transformation plasticity is a result of fluctuations at the micro-scale. However, the author is not aware of investigations of the effects of fluctuations at the macro-scale level.

The meshing could be further improved, particularly the stopping points of each weld pass. Goldak Technologies Inc. is exploring ways to do this, such as domain decomposition with a small domain with a fine mesh and space-time FEM analysis with a graded mesh.

Difficulties Encountered: It would be useful to establish a reference coordinate system and then refer all experimental and computed data to the reference coordinate system.

Sommaire

Validations of Computational Weld Models: Comparison of Residual Stresses

John Goldak; DRDC Atlantic CR 2009-222; R & D pour la défense Canada – Atlantique; août 2010.

Introduction: Lorsque des travaux de soudage sont réalisés afin de réparer des dommages causés par la corrosion ou des accidents, ou pour étanchéiser de nouveau les accès intérieurs de la coque épaisse d'un sous-marin, le comportement en service des structures peut subir les effets de la modification de la géométrie, de la nature et de l'importance des contraintes résiduelles et des propriétés des matériaux. Il existe donc un besoin particulier dans ce domaine, soit l'élaboration d'un outil ayant la capacité d'estimer l'ampleur des changements que provoque le soudage au chapitre de la résistance d'une coque épaisse au gauchissement, à la fatigue et à la rupture.

C'est pourquoi RDDC Atlantique a retenu les services de la société BMT Fleet Technologies Limited afin que celle-ci exécute le soudage de rechargement de deux panneaux rigides. Les structures étaient munies de thermocouples et de jauges de déformation permettant d'enregistrer les variations de température et les déformations durant les étapes de préchauffage, de soudage et de refroidissement. La distorsion de la partie inférieure de la plaque soudée finale a été mesurée et les résultats sont présentés dans le rapport intitulé *Monitoring of Welding Induced Strains during Cladding* [1].

RDDC Atlantique a aussi retenu les services de la société Goldak Technologies Inc. afin que celle-ci exécute la modélisation du procédé de soudage de rechargement utilisé pour fabriquer les deux panneaux rigides. Un résumé des résultats apparaît dans le rapport *Thermo-mechanical modelling of welding induced strains : Numerical validation of the weld build-up process* [2].

Le présent document traite de la comparaison des contraintes résiduelles que présentent les deux panneaux, mesurées par diffraction des neutrons, et de celles calculées au moyen du logiciel *VrWeld*, qui simule la mécanique des procédés de soudage.

Résultats:

1. La simulation de la zone de rechargement mesurant 100 mm sur 100 mm a été réalisée en employant 27 passes de soudure de rechargement, tandis que celle de la zone mesurant 200 mm sur 200 mm a été exécutée en employant 51 passes.
2. On a aussi tenu compte de la composition chimique du métal d'apport, et ce, dans les deux cas étudiés.

3. On a comparé les valeurs des contraintes résiduelles du montage expérimental I, présentant une zone de rechargement de 100 mm sur 100 mm, et du montage expérimental II, présentant une zone de rechargement de 200 mm sur 200 mm, calculées au moyen du logiciel de modélisation de la mécanique des procédés de soudage *VrWeld*, et celles mesurées par diffraction des neutrons. Les contraintes résiduelles mesurées dans les montages expérimentaux l'ont été en des points particuliers des plans longitudinal et transversal.
4. Un examen visuel des graphiques des contraintes résiduelles laisse supposer qu'il existe un certain accord entre les valeurs de contraintes résiduelles mesurées et calculées, mais à la connaissance de l'auteur du présent rapport, il n'existe cependant aucune méthode éprouvée qui permet d'évaluer quantitativement le degré de cet accord ou de la conformité des différents résultats.

Portée: Afin d'effectuer la validation du modèle numérique, il est essentiel de définir une application et de déterminer la sensibilité des résultats de modélisation par rapport à cette application. Le processus visant à déterminer si l'accord obtenu est suffisant pour prendre des décisions de conception particulières serait fonction des applications envisagées.

Recherches futures: D'après l'expérience acquise dans le cadre du présent projet et de projets antérieurs, on peut recommander l'exécution des travaux et activités suivantes :

Un dispositif expérimental (DE) virtuel devrait être élaboré afin de déterminer la sensibilité de la solution par rapport aux paramètres du modèle. Cette approche permettrait d'améliorer l'accord entre les valeurs de contraintes résiduelles mesurées et calculées. Les valeurs calculées des contraintes longitudinales dans le métal d'apport (métal de soudure) semblent être supérieures à celles mesurées. Ces contraintes résiduelles de traction plus élevées dans le métal d'apport pourraient constituer la cause des contraintes résiduelles de compression plus élevées observées dans la zone inférieure adjacente. Ces faits laissent supposer qu'il serait utile de réaliser une analyse de DE afin de calculer la sensibilité aux changements de la contrainte d'écoulement dans les phases de martensite et de bainite et de déterminer s'il est ainsi possible d'améliorer l'accord entre les valeurs mesurées et calculées des contraintes résiduelles.

Il faudrait analyser les effets de la martensite sur le processus de recuit afin de réduire la dureté de la phase martensitique qui est formée dans une passe de soudure par une passe ultérieure. Une telle réduction de la dureté semble indiquer que la contrainte d'écoulement de la martensite pourrait être réduite, par rapport à une valeur de quelque 900 MPa pour la martensite n'ayant pas subi un recuit. Si un modèle du processus de recuit de la martensite peut être élaboré, il pourrait être intégré au modèle informatique.

Les mesures de la dureté de la plaque laissent supposer que cette propriété varie grandement dans l'espace, c.-à-d. qu'elle est inhomogène. Il serait intéressant d'étudier les effets de

ces variations sur les contraintes résiduelles. La plasticité de transformation découle de variations qui se produisent à l'échelle du micromètre. À la connaissance de l'auteur du présent rapport, il n'existe cependant aucune étude portant sur les effets des variations à l'échelle macroscopique.

La qualité du maillage pourrait être améliorée, particulièrement aux points d'interruption de chaque passe de soudure. La société Goldak Technologies Inc. examine actuellement des moyens d'atteindre cet objectif, par exemple en employant un domaine de petites dimensions à maillage fin et l'analyse FEM (modèle par éléments finis) dans l'espace et le temps avec maillage dimensionné.

Problèmes rencontrés: Il serait utile d'établir un système de coordonnées de référence et d'exprimer toutes les données expérimentales et calculées en fonction de ce système.

This page intentionally left blank.

Table of contents

Abstract i

Résumé i

Executive summary iii

Sommaire v

Table of contents ix

List of figures x

List of tables xiv

1 Modelling the Structures 1

1.1 Thermal Analysis 4

1.2 Chemical Compositions 4

2 Experimental Measurements 5

3 Influence of Weld Composition 7

4 Comparison of Measured and Computed Residual stress 10

5 Discussion of Comparison of Measured and Computed Residual Stress 29

6 Recommendations and Future Work 31

References 32

Distribution List 33

List of figures

Figure 1: A cross-section of the fine mesh of the 100 × 100 overlay is shown. . . . 1

Figure 2: A cross-section of the fine mesh of the 100 × 100 overlay is shown. The filler metal cross-sections are coloured. 1

Figure 3: A cross-section of the fine mesh of the 200 × 200 overlay is shown. . . . 2

Figure 4: A cross-section of the fine mesh of the 200 × 200 overlay is shown. . . . 2

Figure 5: A view of the fine mesh of the 100 × 100 overlay structure is shown. The green ball represents a virtual thermocouple. The pairs of white balls represent virtual strain gauges. 3

Figure 6: The small experimental calibration panel showing the approximate location of the two through thickness planes used to acquire the residual stress measurements. Along the longitudinally oriented plane, the measurements extended across the whole weld panel, while for the transverse plane, only half of the build-up panel was measured. Measurements were acquired in the longitudinal, transverse and normal direction at geometrically similar positions. 5

Figure 7: The large experimental calibration panel showing the approximate location of the two through thickness planes used to acquire the residual stress measurements. Along the longitudinally oriented plane, the measurements extended across the whole weld panel, while for the transverse plane, only half of the build-up panel was measured. 6

Figure 8: Influence of the weld metal chemistry on the computed residual stresses (100 × 100 Longitudinal Stress Component Across the Weld) 7

Figure 9: Influence of the weld metal chemistry on the computed residual stresses (100 × 100 Transverse Stress Component Across the Weld) 8

Figure 10: Influence of the weld metal chemistry on the computed residual stresses (100 × 100 Normal Stress Component Across the Weld) 9

Figure 11: The images are for longitudinal stress on the small panel in the plane parallel to the welding direction. In the top image the FEM data is plotted with linear interpolation between data points on a cut-plane mesh in the 3D mesh used to solve for stresses. In the remaining images data is plotted using linear interpolation between data points on the grid of points used to measure residual stresses. The grid points are shown as black disks. The second image from top shows the measured data. The third image from the top shows the FEM data mapped to the grid. The bottom image shows the difference of the measured data from the FEM data. 11

Figure 12: The images are for transverse stress on the small panel in the plane parallel to the welding direction. In the top image the FEM data is plotted with linear interpolation between data points on a cut-plane mesh in the 3D mesh used to solve for stresses. In the remaining images data is plotted using linear interpolation between data points on the grid of points used to measure residual stresses. The grid points are shown as black disks. The second image from top shows the measured data. The third image from the top shows the FEM data mapped to the grid. The bottom image shows the difference of the measured data from the FEM data. 12

Figure 13: The images are for normal stress on the small panel in the plane parallel to the welding direction. In the top image the FEM data is plotted with linear interpolation between data points on a cut-plane mesh in the 3D mesh used to solve for stresses. In the remaining images data is plotted using linear interpolation between data points on the grid of points used to measure residual stresses. The grid points are shown as black disks. The second image from top shows the measured data. The third image from the top shows the FEM data mapped to the grid. The bottom image shows the difference of the measured data from the FEM data. . . 13

Figure 14: The images are for longitudinal stress on the small panel in the plane perpendicular to the welding direction. In the top image the FEM data is plotted with linear interpolation between data points on a cut-plane mesh in the 3D mesh used to solve for stresses. In the remaining images data is plotted using linear interpolation between data points on the grid of points used to measure residual stresses. The grid points are shown as black disks. The second image from top shows the measured data. The third image from the top shows the FEM data mapped to the grid. The bottom image shows the difference of the measured data from the FEM data. 14

Figure 15: The images are for transverse stress on the small panel in the plane perpendicular to the welding direction. In the top image the FEM data is plotted with linear interpolation between data points on a cut-plane mesh in the 3D mesh used to solve for stresses. In the remaining images data is plotted using linear interpolation between data points on the grid of points used to measure residual stresses. The grid points are shown as black disks. The second image from top shows the measured data. The third image from the top shows the FEM data mapped to the grid. The bottom image shows the difference of the measured data from the FEM data. 15

Figure 16: The images are for normal stress on the small panel in the plane perpendicular to the welding direction. In the top image the FEM data is plotted with linear interpolation between data points on a cut-plane mesh in the 3D mesh used to solve for stresses. In the remaining images data is plotted using linear interpolation between data points on the grid of points used to measure residual stresses. The grid points are shown as black disks. The second image from top shows the measured data. The third image from the top shows the FEM data mapped to the grid. The bottom image shows the difference of the measured data from the FEM data. 16

Figure 17: The images are for longitudinal stress on the large panel in the plane parallel to the welding direction. In the top image the FEM data is plotted with linear interpolation between data points on a cut-plane mesh in the 3D mesh used to solve for stresses. In the remaining images data is plotted using linear interpolation between data points on the grid of points used to measure residual stresses. The grid points are shown as black disks. The second image from top shows the measured data. The third image from the top shows the FEM data mapped to the grid. The bottom image shows the difference of the measured data from the FEM data. 17

Figure 18: The images are for transverse stress on the large panel in the plane parallel to the welding direction. In the top image the FEM data is plotted with linear interpolation between data points on a cut-plane mesh in the 3D mesh used to solve for stresses. In the remaining images data is plotted using linear interpolation between data points on the grid of points used to measure residual stresses. The grid points are shown as black disks. The second image from top shows the measured data. The third image from the top shows the FEM data mapped to the grid. The bottom image shows the difference of the measured data from the FEM data. 18

Figure 19: The images are for normal stress on the large panel in the plane parallel to the welding direction. In the top image the FEM data is plotted with linear interpolation between data points on a cut-plane mesh in the 3D mesh used to solve for stresses. In the remaining images data is plotted using linear interpolation between data points on the grid of points used to measure residual stresses. The grid points are shown as black disks. The second image from top shows the measured data. The third image from the top shows the FEM data mapped to the grid. The bottom image shows the difference of the measured data from the FEM data. . . . 19

Figure 20: Measured (top) and computed (bottom) longitudinal residual stress in the small panel in the plane parallel to the weld direction is shown. . . . 20

Figure 21: Measured (top) and computed (bottom) transverse residual stress in the small panel in the plane parallel to the weld direction is shown. 21

Figure 22: Measured (top) and computed (bottom) normal residual stress in the small panel in the plane parallel to the weld direction is shown. 22

Figure 23: Measured (top) and computed (bottom) longitudinal residual stress in the small panel in the plane normal to the weld direction is shown. . . . 23

Figure 24: Measured (top) and computed (bottom) transverse residual stress in the small panel in the plane normal to the weld direction is shown. 24

Figure 25: Measured (top) and computed (bottom) normal residual stress in the small panel in the plane normal to the weld direction is shown. 25

Figure 26: Measured (top) and computed (bottom) longitudinal residual stress in the large panel in the plane parallel to the weld direction is shown. . . . 26

Figure 27: Measured (top) and computed (bottom) transverse residual stress in the large panel in the plane parallel to the weld direction is shown. 27

Figure 28: Measured (top) and computed (bottom) normal residual stress in the large panel in the plane parallel to the weld direction is shown. 28

Figure 29: The difference between the computed and measured transverse residual stress in the large panel in the plane parallel to the weld direction is shown. Compare to Fig. 27. 30

List of tables

Table 1: Chemical composition of parent and consumable materials (in wt%) . . . 4

1 Modelling the Structures

The fine mesh of the 100×100 overlay has 15,606 elements and 24,727 nodes. The fine mesh of the 200×200 overlay has 50,808 elements and 69,627 nodes. The coarse mesh of the 200×200 overlay has 21,978 elements and 32,880 nodes. The fine meshes are considered to be very high quality meshes. The cross-section of each filler metal weld pass had from 6 to 15 brick elements. The mesh for the region being welded including the filler metal were meshed with 8-node bricks. The complement of the region being welded was meshed with 6-node prism and 8-node brick elements. The meshing was done in *VrSuite*. Various views of these meshes are shown in Figures 1-5.

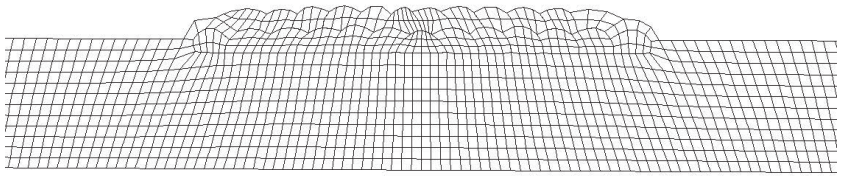

Figure 1: *A cross-section of the fine mesh of the* 100×100 *overlay is shown.*

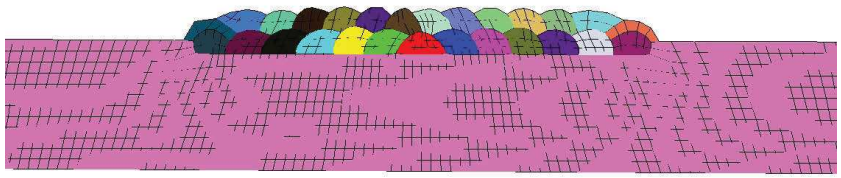

Figure 2: *A cross-section of the fine mesh of the* 100×100 *overlay is shown. The filler metal cross-sections are coloured.*

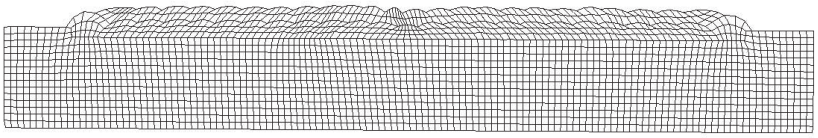

Figure 3: *A cross-section of the fine mesh of the* 200×200 *overlay is shown.*

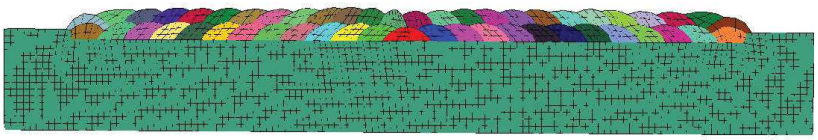

Figure 4: *A cross-section of the fine mesh of the* 200×200 *overlay is shown.*

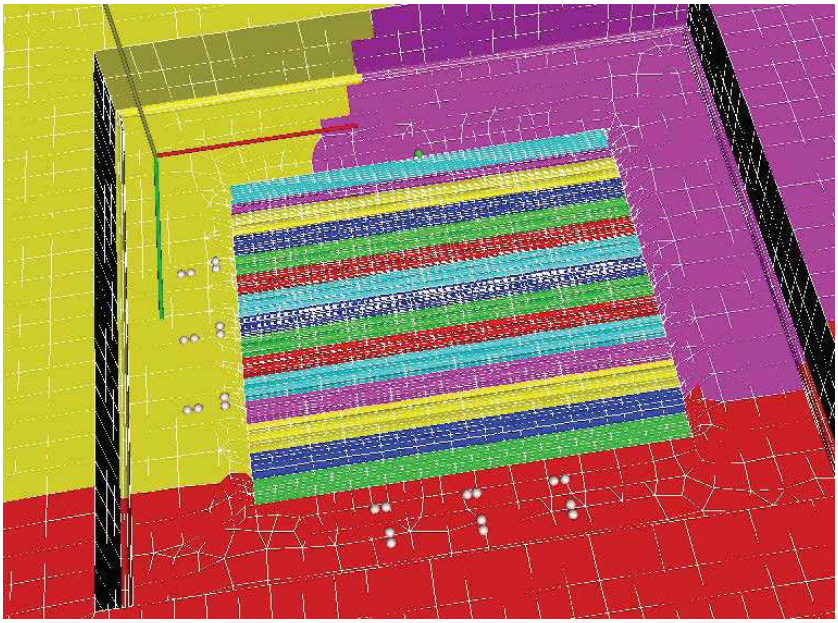

Figure 5: *A view of the fine mesh of the* 100×100 *overlay structure is shown. The green ball represents a virtual thermocouple. The pairs of white balls represent virtual strain gauges.*

1.1 Thermal Analysis

Weld passes were deposited in the depressions in a symmetrical sequence which incrementally increased the clad width and hence balances the welding induced strain. The plate material was HY80 and the filler metal Fortrex AWS E9016. During the welding process transient temperatures were recorded with thermocouples and transient strains with strain gauges. After welding and cool-down to room temperature, the distortion on the bottom of each plate was measured along with through-thickness residual stress measurements. CR 2008-283 [2] provides further details of the analysis procedure.

1.2 Chemical Compositions

Two variations in the chemical compositions were examined. In the first case both the base metal and weld filler metal utilized the parent metal composition listed in Table 1, while in the second case, the weld metal utilized the as-deposited chemical composition. .

Table 1: *Chemical composition of parent and consumable materials (in wt%)*

Composition	C	Mn	Si	S	P	Ni	Cr	Mo
Parent metal	0.14	0.27	0.15	0.002	0.006	2.2	1.1	0.25
Weld metal as-deposited	0.08	1.3	0.17	0.002	0.009	1.1	0.23	0.18

2 Experimental Measurements

McLaughlin [8] obtained neutron diffraction measurements from the weld built-up panels along the four planes illustrated in Figure 6 and 7 for the small and large weld patches, respectively. The experimental residual stresses were measured on a 6×24 grid on a longitudinal plane and a 7×13 grid on transverse plane on the small weld patch and a 7×13 grid on a longitudinal plane on the large weld patch. These measurement locations are represented by red dots in Figures 6 and 7.

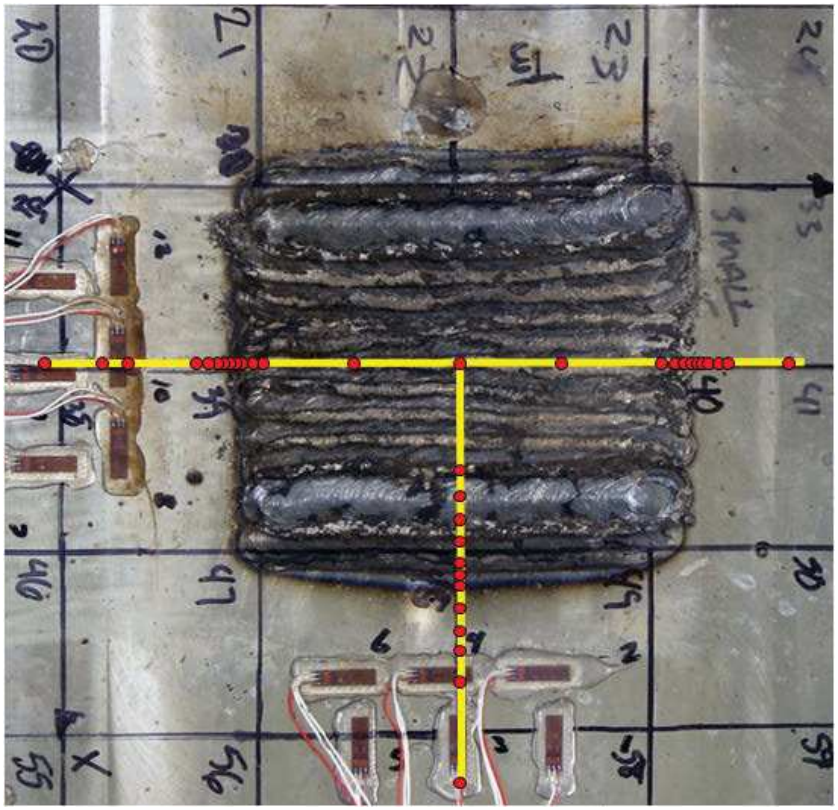

Figure 6: *The small experimental calibration panel showing the approximate location of the two through thickness planes used to acquire the residual stress measurements. Along the longitudinally oriented plane, the measurements extended across the whole weld panel, while for the transverse plane, only half of the build-up panel was measured. Measurements were acquired in the longitudinal, transverse and normal direction at geometrically similar positions.*

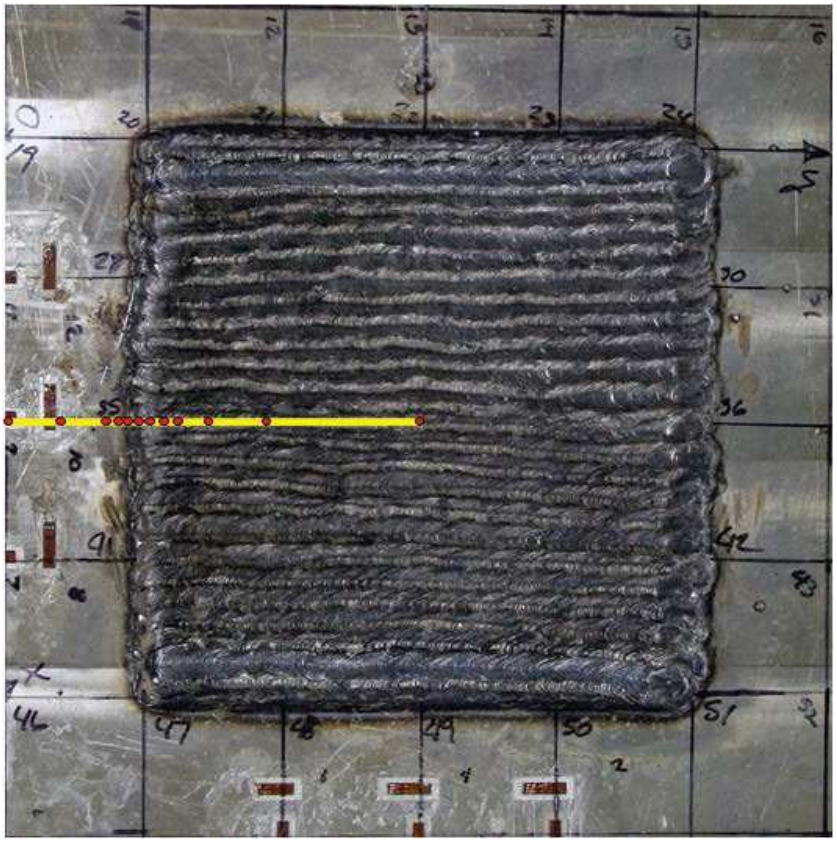

Figure 7: *The large experimental calibration panel showing the approximate location of the two through thickness planes used to acquire the residual stress measurements. Along the longitudinally oriented plane, the measurements extended across the whole weld panel, while for the transverse plane, only half of the build-up panel was measured.*

3 Influence of Weld Composition

The influence that the weld metal composition has on the computed residual stresses are examined in Figure 8 to 10. These compare the longitudinal, transverse and normal stress components along a transverse weld section on the 100×100 weld patch (See Figure 6). In all cases subtle changes in the residual stress field are calculate demonstrating that the influence of chemical composition on mechanical properties can be computed.

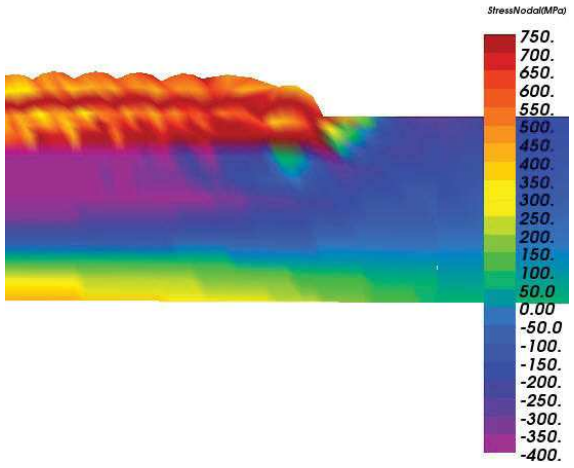

(a) Weld uses base composition

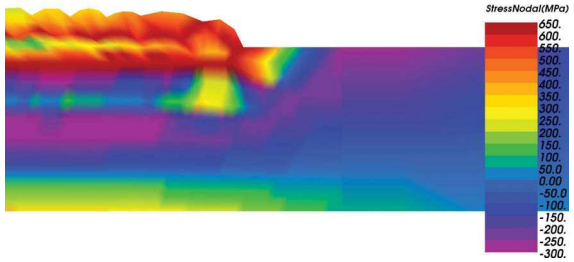

(b) As-deposited composition

Figure 8: *Influence of the weld metal chemistry on the computed residual stresses (*100×100 *Longitudinal Stress Component Across the Weld)*

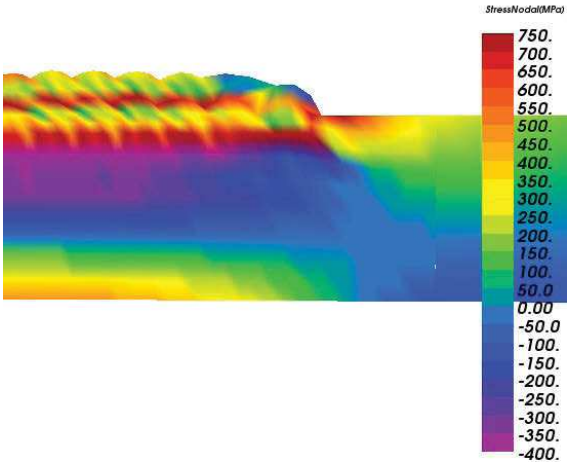

(a) Weld uses base composition

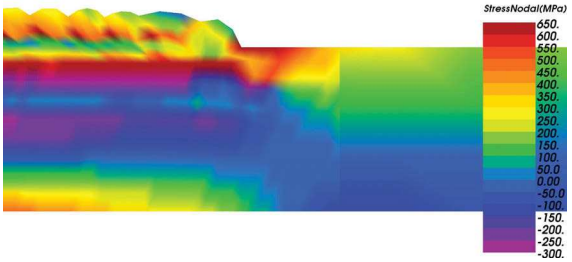

(b) As-deposited composition

Figure 9: *Influence of the weld metal chemistry on the computed residual stresses (*100 $\times$ 100 *Transverse Stress Component Across the Weld)*

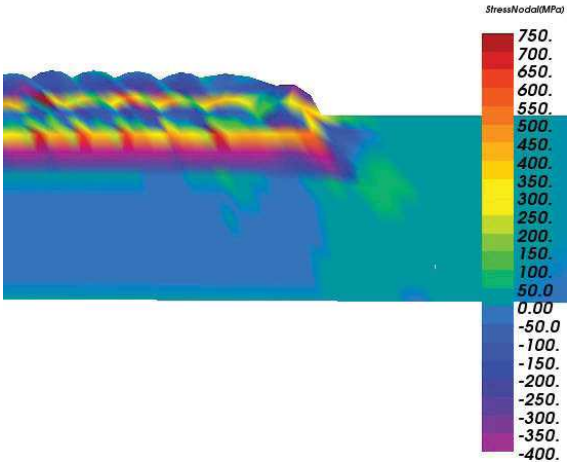

(a) Weld uses base composition

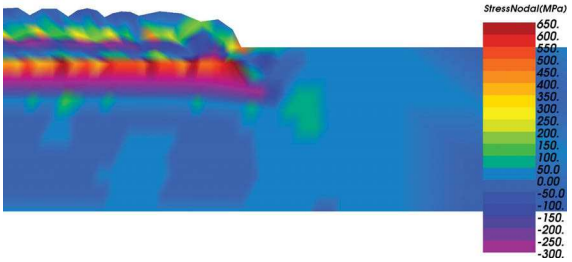

(b) As-deposited composition

Figure 10: *Influence of the weld metal chemistry on the computed residual stresses (*100 $\times$ 100 *Normal Stress Component Across the Weld)*

4 Comparison of Measured and Computed Residual stress

The longitudinal, transverse and normal residual stress is measured at points on a coarse grid in a longitudinal and a transverse plane in the small patch (Figure 6) and in a longitudinal plane in the large patch (Figure 7). The images of the measured stress distribution are shown in the second image from the top in Figures 11 to 19. These images were computed by interpolating data from this coarse grid to the the pixels in the image.

The longitudinal, transverse and normal residual stress is computed at points in a much finer FEM mesh. The images of the stress distribution are computed by interpolating data from this fine FEM mesh to the the pixels in the top image on Figures 11 to 19. Note these images do not use interpolation on the coarse grid to the pixels in the image.

An FEM mesh was created in which the nodes correspond to data points used to measure the residual stress. Data from the fine FEM mesh was mapped to these coarse grid points and then interpolated to image pixels to create the third from the top image in on Figures 11 to 19 . These images were computed by interpolating data from this coarse grid to the the pixels in the image.

The bottom image in Figures 11 to 19 are the difference between the measured and computed stress at the grid points which is interpolated to pixels to create the image. These images were computed by interpolating data from this coarse grid to the the pixels in the image.

Figures 20 to 25 show line plots for measured and computed stresses on each line of the associated coarse grid in the small panel. Figures 26 to 28 show line plots for measured and computed stresses on each line of the associated coarse grid in the large panel.

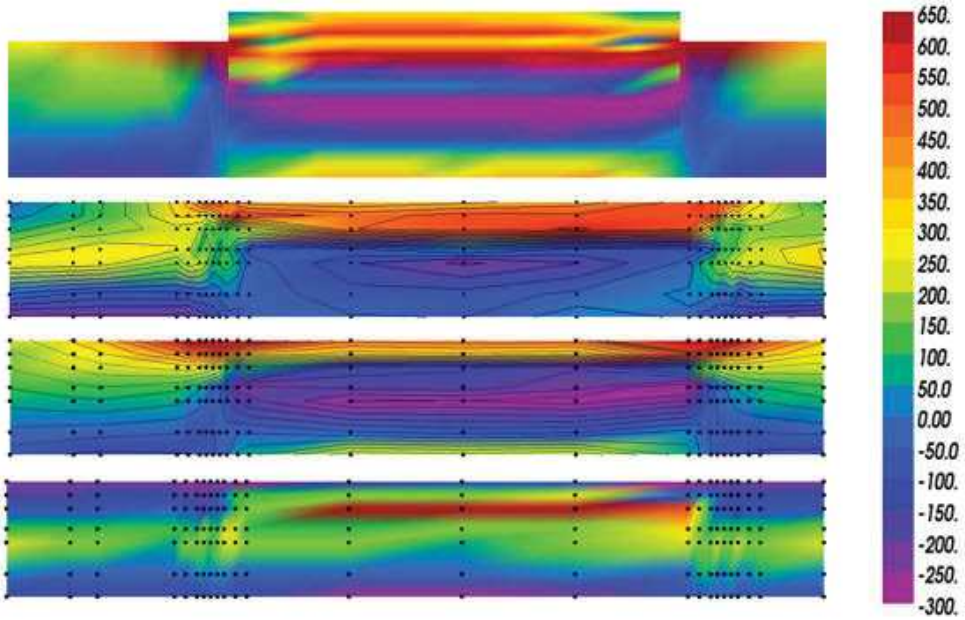

Figure 11: *The images are for longitudinal stress on the small panel in the plane parallel to the welding direction. In the top image the FEM data is plotted with linear interpolation between data points on a cut-plane mesh in the 3D mesh used to solve for stresses. In the remaining images data is plotted using linear interpolation between data points on the grid of points used to measure residual stresses. The grid points are shown as black disks. The second image from top shows the measured data. The third image from the top shows the FEM data mapped to the grid. The bottom image shows the difference of the measured data from the FEM data.*

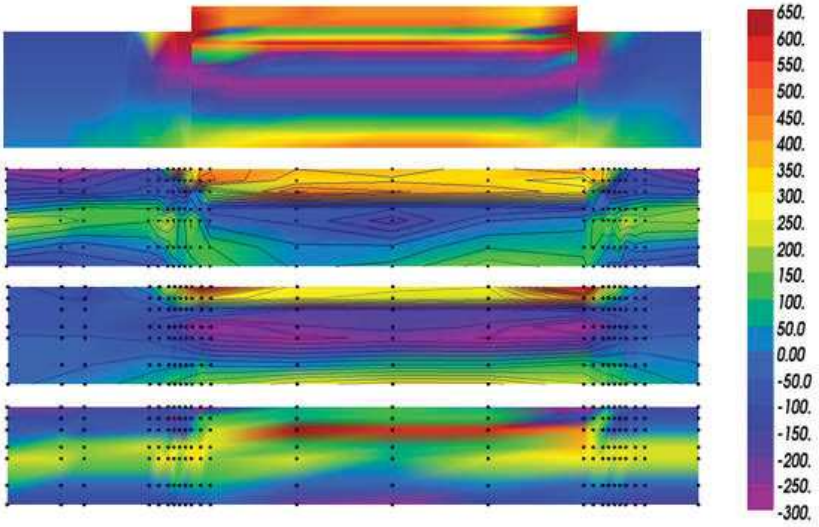

Figure 12: *The images are for transverse stress on the small panel in the plane parallel to the welding direction. In the top image the FEM data is plotted with linear interpolation between data points on a cut-plane mesh in the 3D mesh used to solve for stresses. In the remaining images data is plotted using linear interpolation between data points on the grid of points used to measure residual stresses. The grid points are shown as black disks. The second image from top shows the measured data. The third image from the top shows the FEM data mapped to the grid. The bottom image shows the difference of the measured data from the FEM data.*

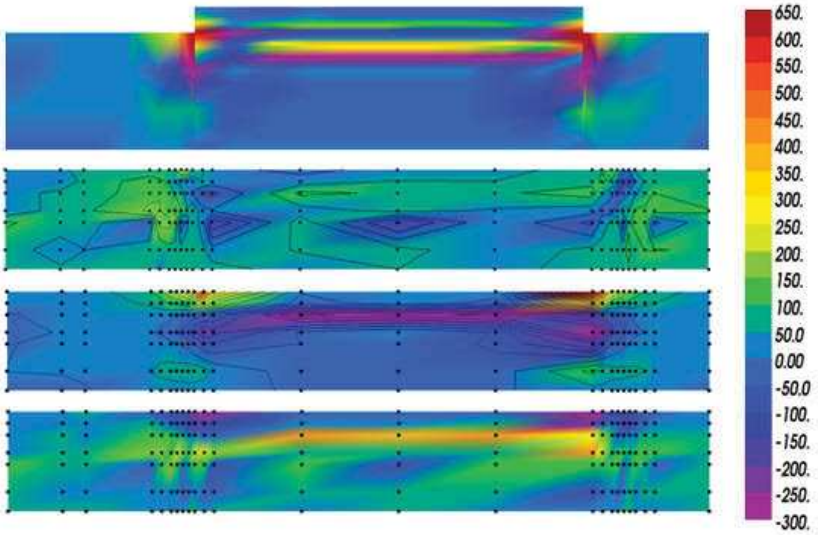

Figure 13: *The images are for normal stress on the small panel in the plane parallel to the welding direction. In the top image the FEM data is plotted with linear interpolation between data points on a cut-plane mesh in the 3D mesh used to solve for stresses. In the remaining images data is plotted using linear interpolation between data points on the grid of points used to measure residual stresses. The grid points are shown as black disks. The second image from top shows the measured data. The third image from the top shows the FEM data mapped to the grid. The bottom image shows the difference of the measured data from the FEM data.*

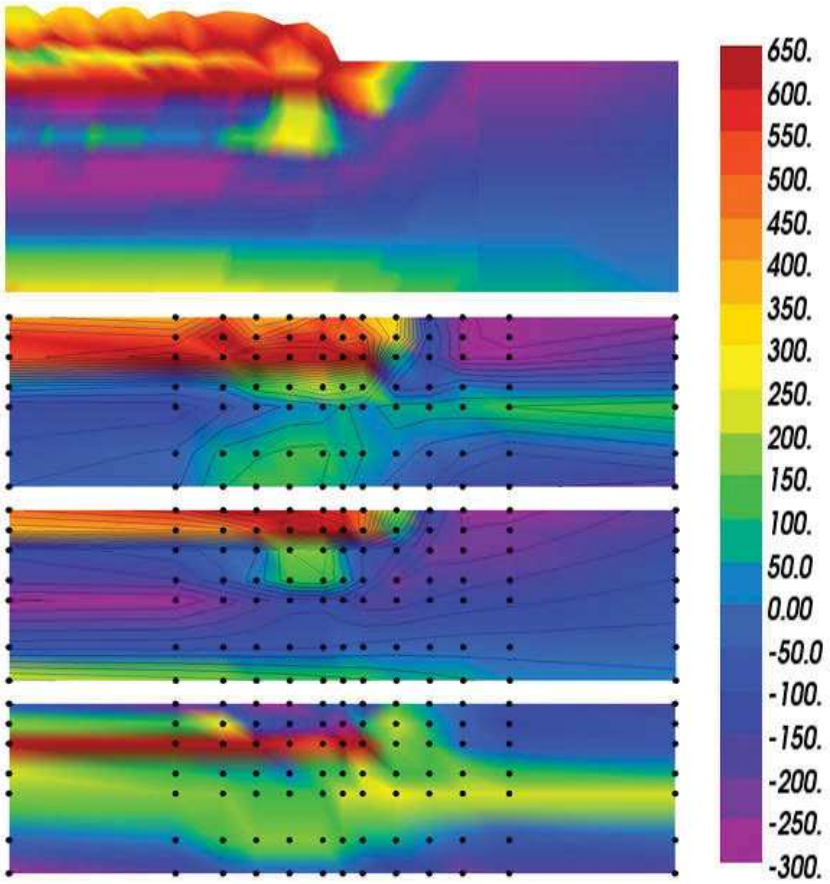

Figure 14: *The images are for longitudinal stress on the small panel in the plane perpendicular to the welding direction. In the top image the FEM data is plotted with linear interpolation between data points on a cut-plane mesh in the 3D mesh used to solve for stresses. In the remaining images data is plotted using linear interpolation between data points on the grid of points used to measure residual stresses. The grid points are shown as black disks. The second image from top shows the measured data. The third image from the top shows the FEM data mapped to the grid. The bottom image shows the difference of the measured data from the FEM data.*

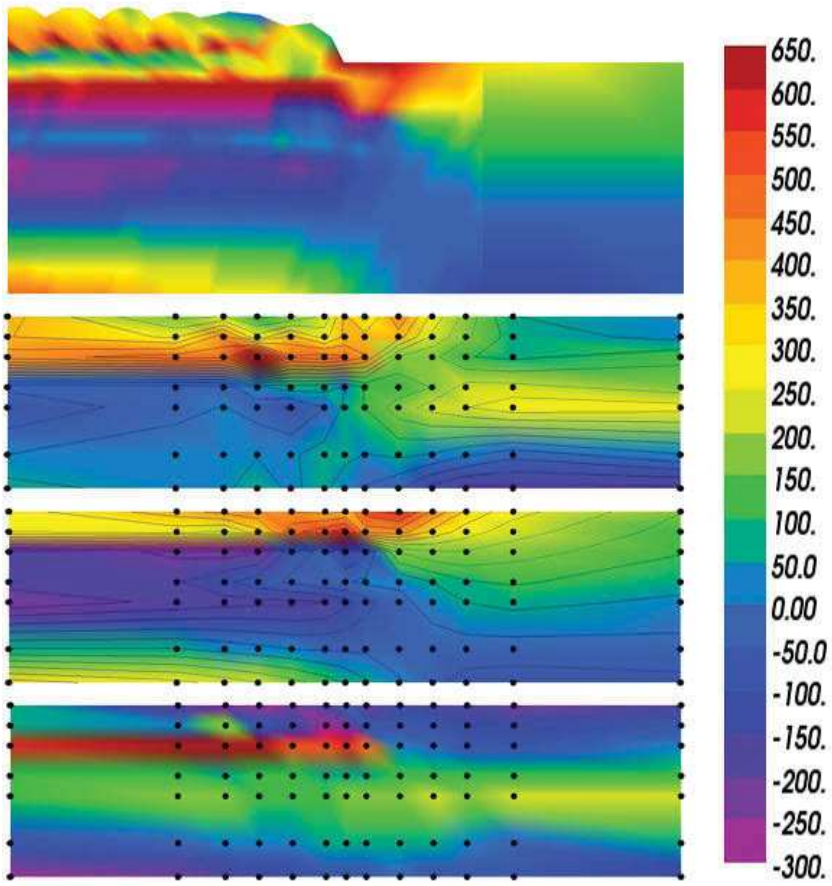

Figure 15: *The images are for transverse stress on the small panel in the plane perpendicular to the welding direction. In the top image the FEM data is plotted with linear interpolation between data points on a cut-plane mesh in the 3D mesh used to solve for stresses. In the remaining images data is plotted using linear interpolation between data points on the grid of points used to measure residual stresses. The grid points are shown as black disks. The second image from top shows the measured data. The third image from the top shows the FEM data mapped to the grid. The bottom image shows the difference of the measured data from the FEM data.*

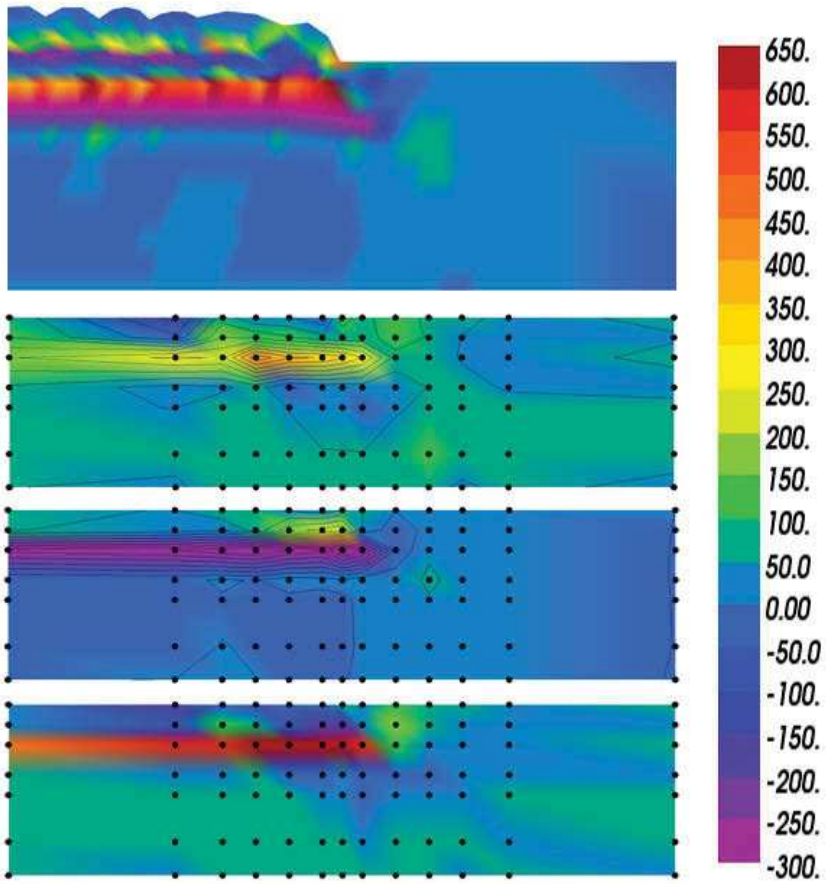

Figure 16: *The images are for normal stress on the small panel in the plane perpendicular to the welding direction. In the top image the FEM data is plotted with linear interpolation between data points on a cut-plane mesh in the 3D mesh used to solve for stresses. In the remaining images data is plotted using linear interpolation between data points on the grid of points used to measure residual stresses. The grid points are shown as black disks. The second image from top shows the measured data. The third image from the top shows the FEM data mapped to the grid. The bottom image shows the difference of the measured data from the FEM data.*

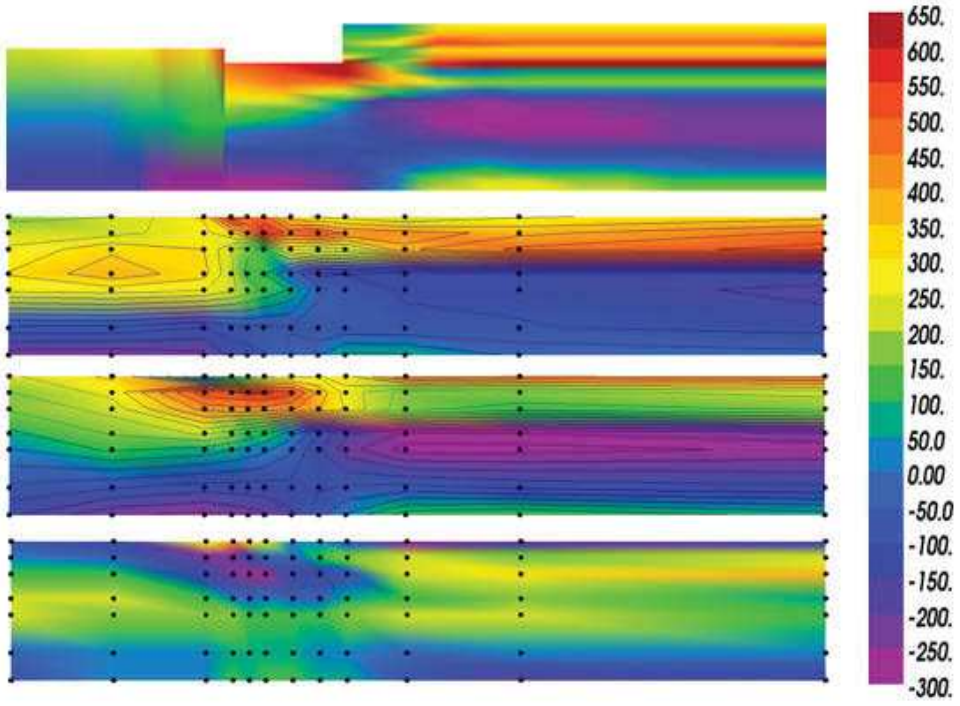

Figure 17: *The images are for longitudinal stress on the large panel in the plane parallel to the welding direction. In the top image the FEM data is plotted with linear interpolation between data points on a cut-plane mesh in the 3D mesh used to solve for stresses. In the remaining images data is plotted using linear interpolation between data points on the grid of points used to measure residual stresses. The grid points are shown as black disks. The second image from top shows the measured data. The third image from the top shows the FEM data mapped to the grid. The bottom image shows the difference of the measured data from the FEM data.*

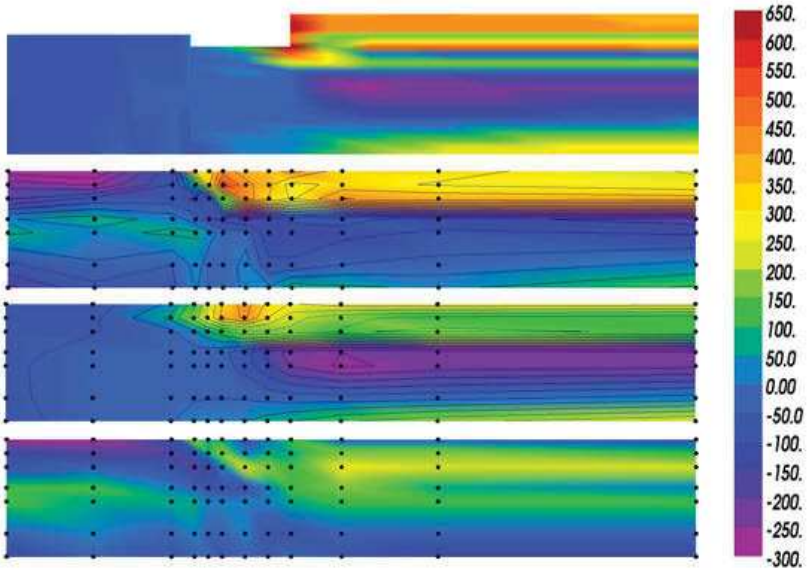

Figure 18: *The images are for transverse stress on the large panel in the plane parallel to the welding direction. In the top image the FEM data is plotted with linear interpolation between data points on a cut-plane mesh in the 3D mesh used to solve for stresses. In the remaining images data is plotted using linear interpolation between data points on the grid of points used to measure residual stresses. The grid points are shown as black disks. The second image from top shows the measured data. The third image from the top shows the FEM data mapped to the grid. The bottom image shows the difference of the measured data from the FEM data.*

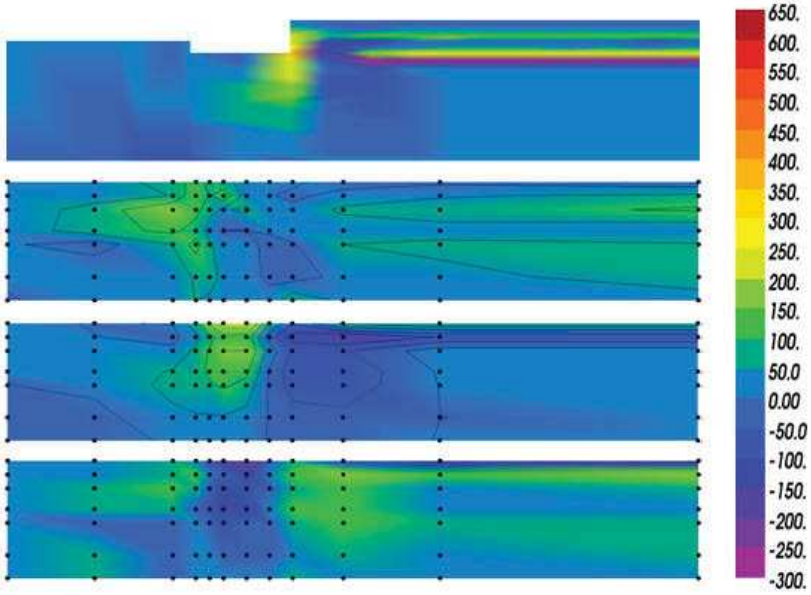

Figure 19: *The images are for normal stress on the large panel in the plane parallel to the welding direction. In the top image the FEM data is plotted with linear interpolation between data points on a cut-plane mesh in the 3D mesh used to solve for stresses. In the remaining images data is plotted using linear interpolation between data points on the grid of points used to measure residual stresses. The grid points are shown as black disks. The second image from top shows the measured data. The third image from the top shows the FEM data mapped to the grid. The bottom image shows the difference of the measured data from the FEM data.*

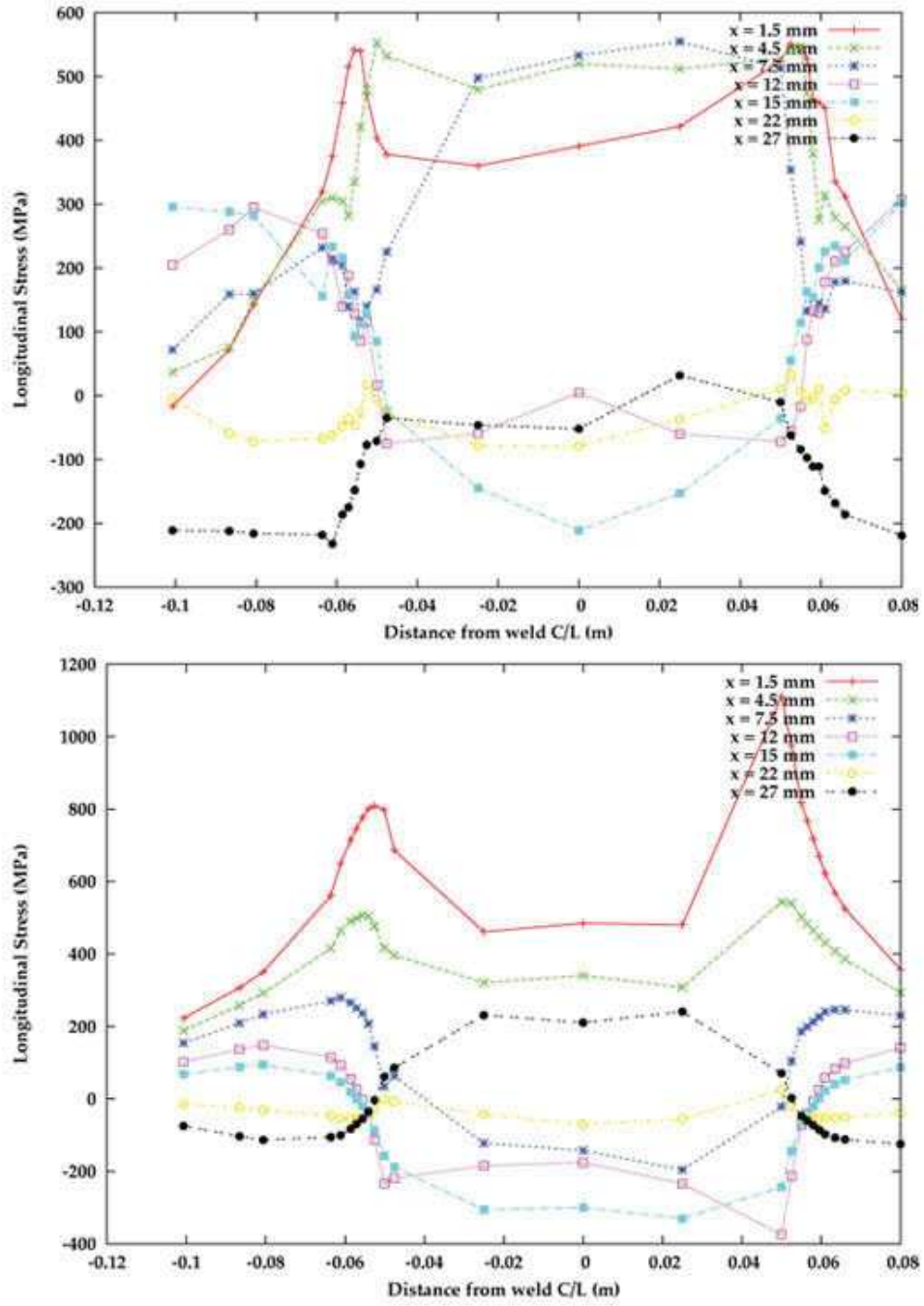

Figure 20: *Measured (top) and computed (bottom) longitudinal residual stress in the small panel in the plane parallel to the weld direction is shown.*

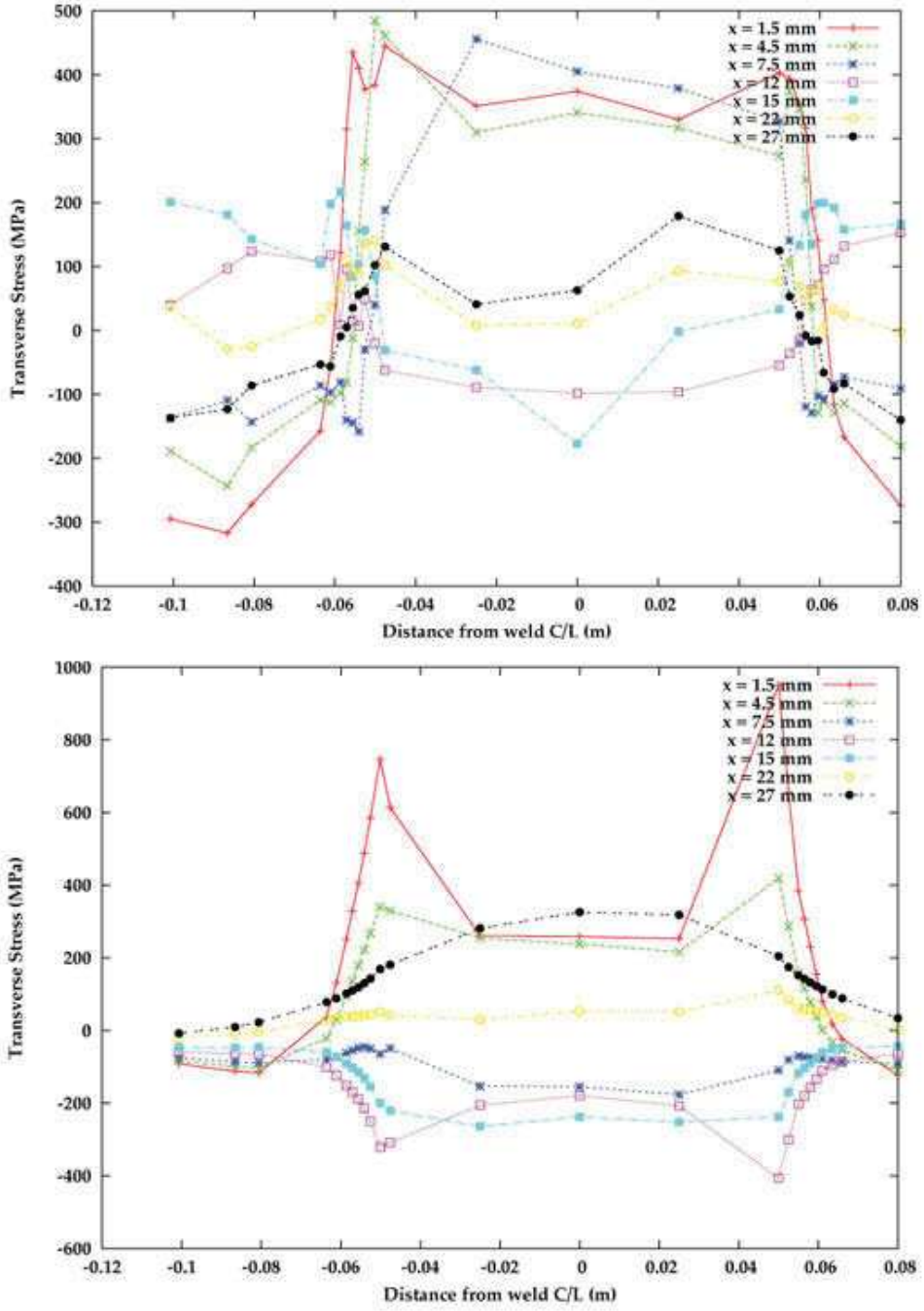

Figure 21: *Measured (top) and computed (bottom) transverse residual stress in the small panel in the plane parallel to the weld direction is shown.*

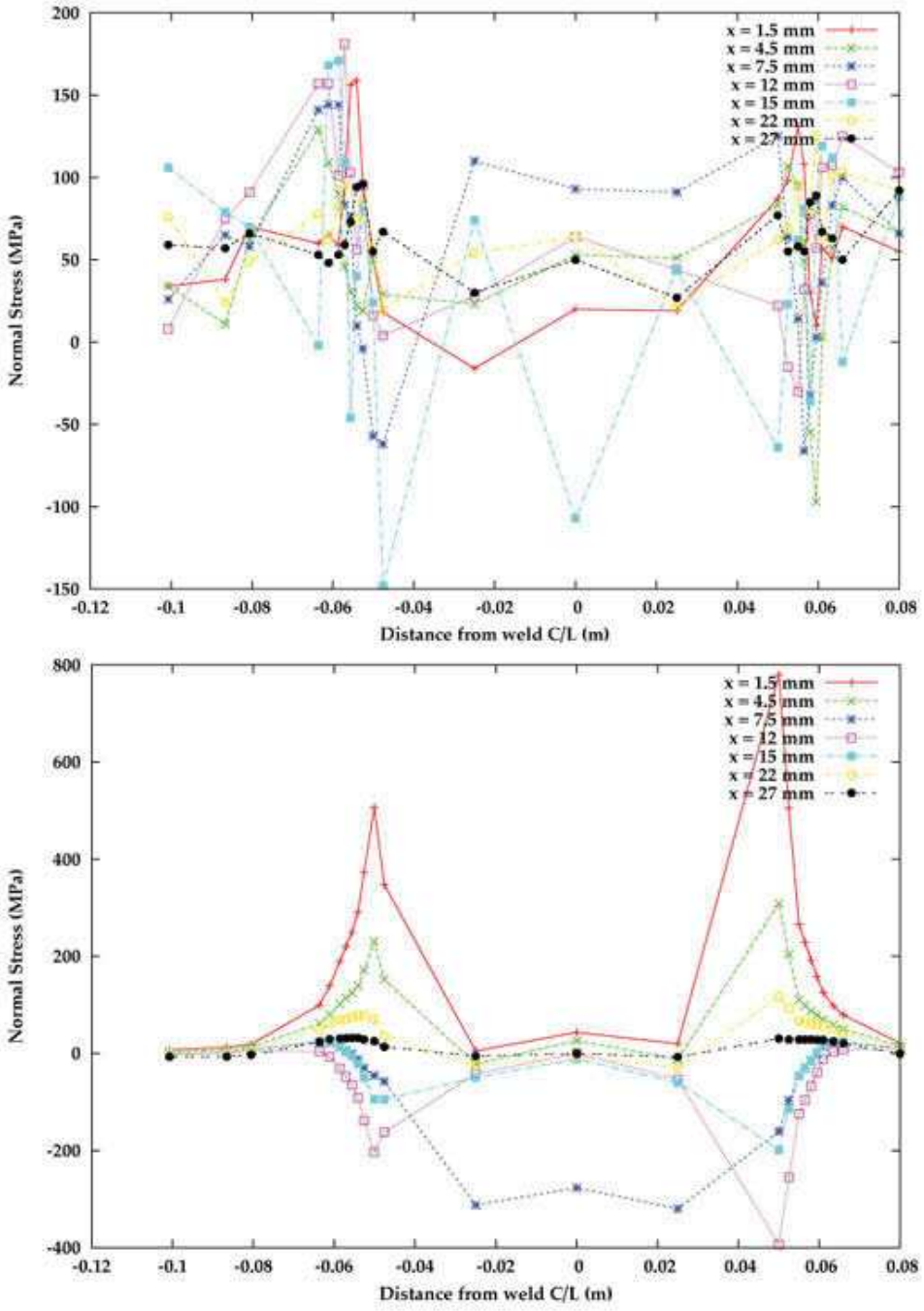

Figure 22: *Measured (top) and computed (bottom) normal residual stress in the small panel in the plane parallel to the weld direction is shown.*

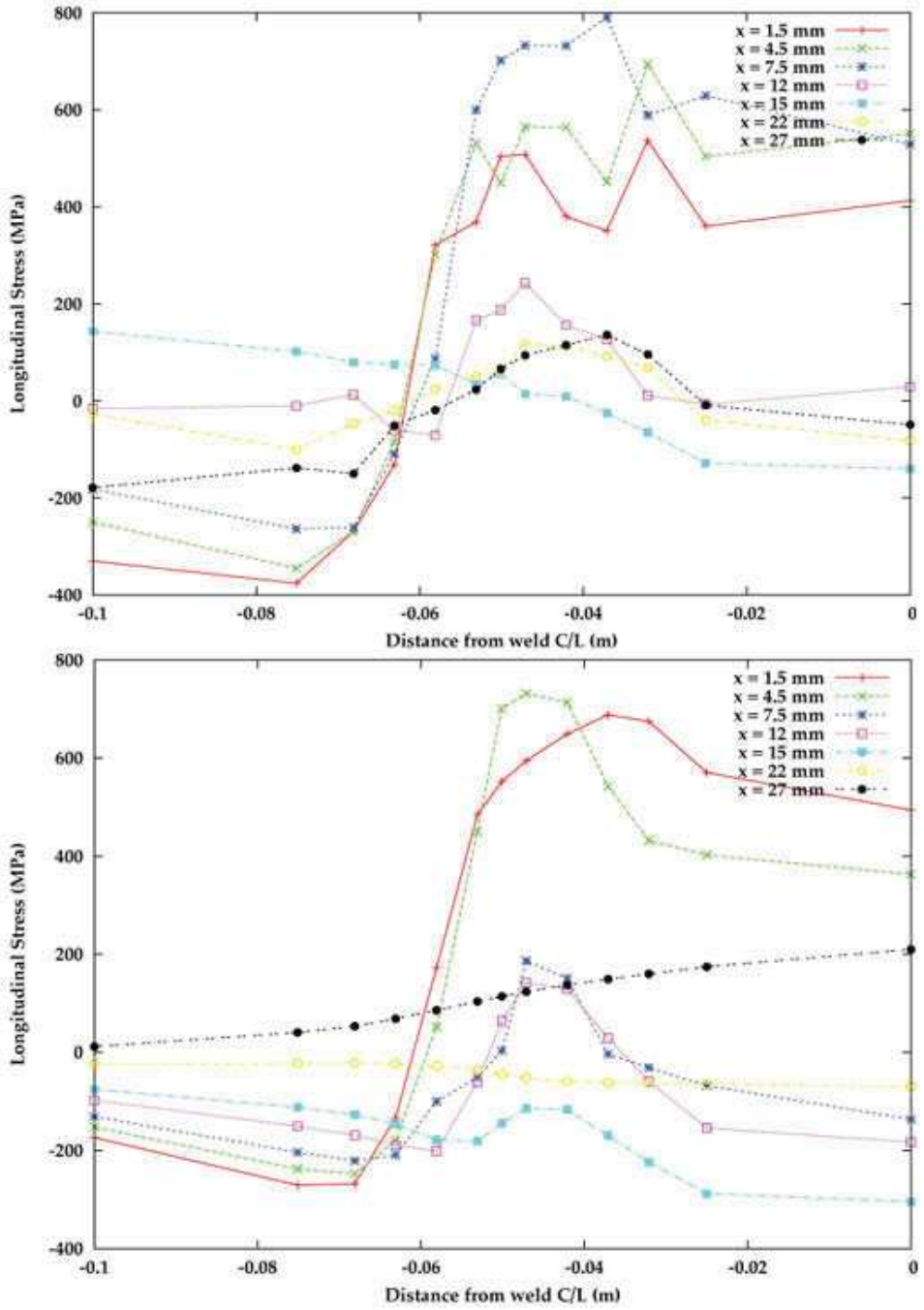

Figure 23: *Measured (top) and computed (bottom) longitudinal residual stress in the small panel in the plane normal to the weld direction is shown.*

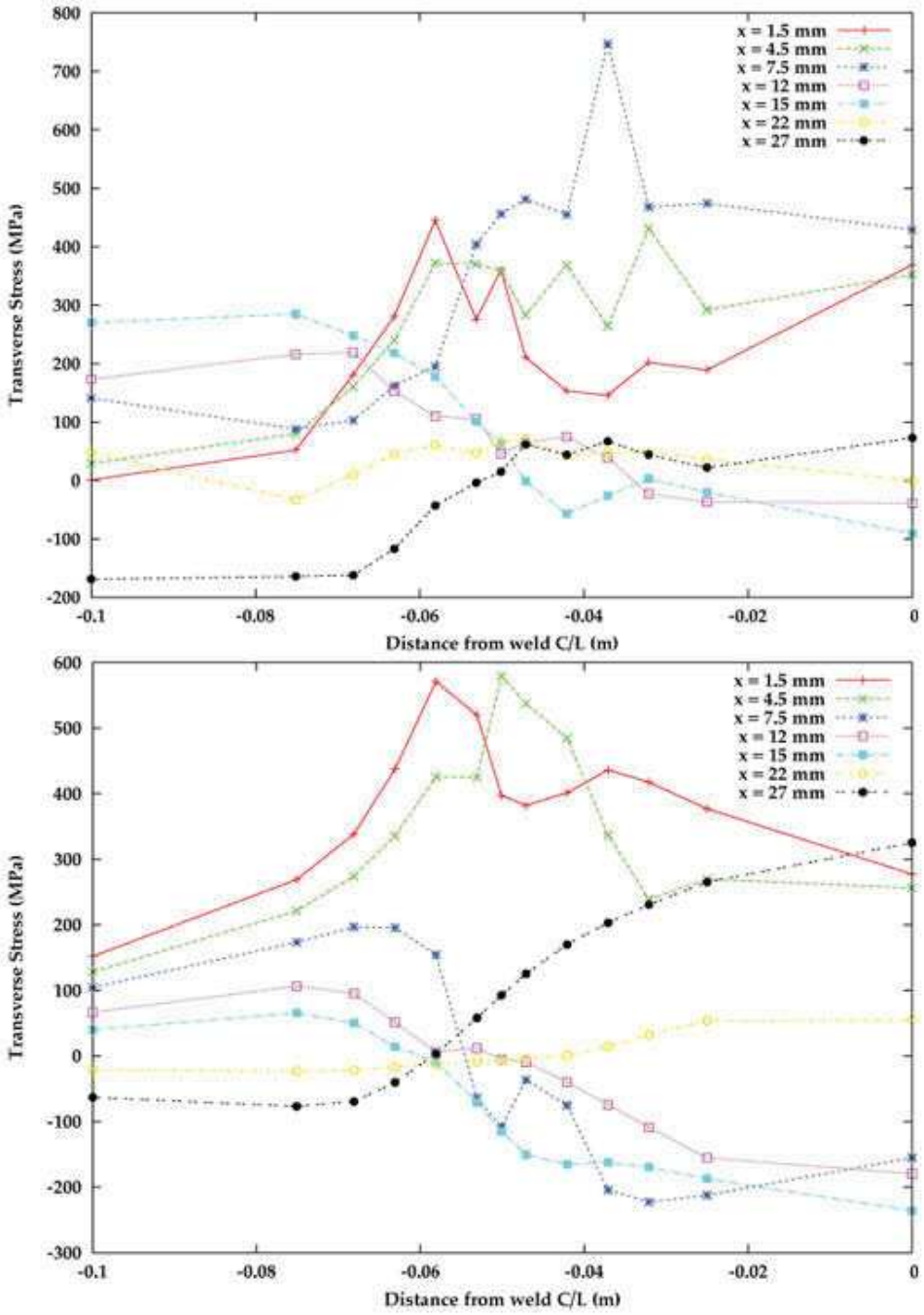

Figure 24: *Measured (top) and computed (bottom) transverse residual stress in the small panel in the plane normal to the weld direction is shown.*

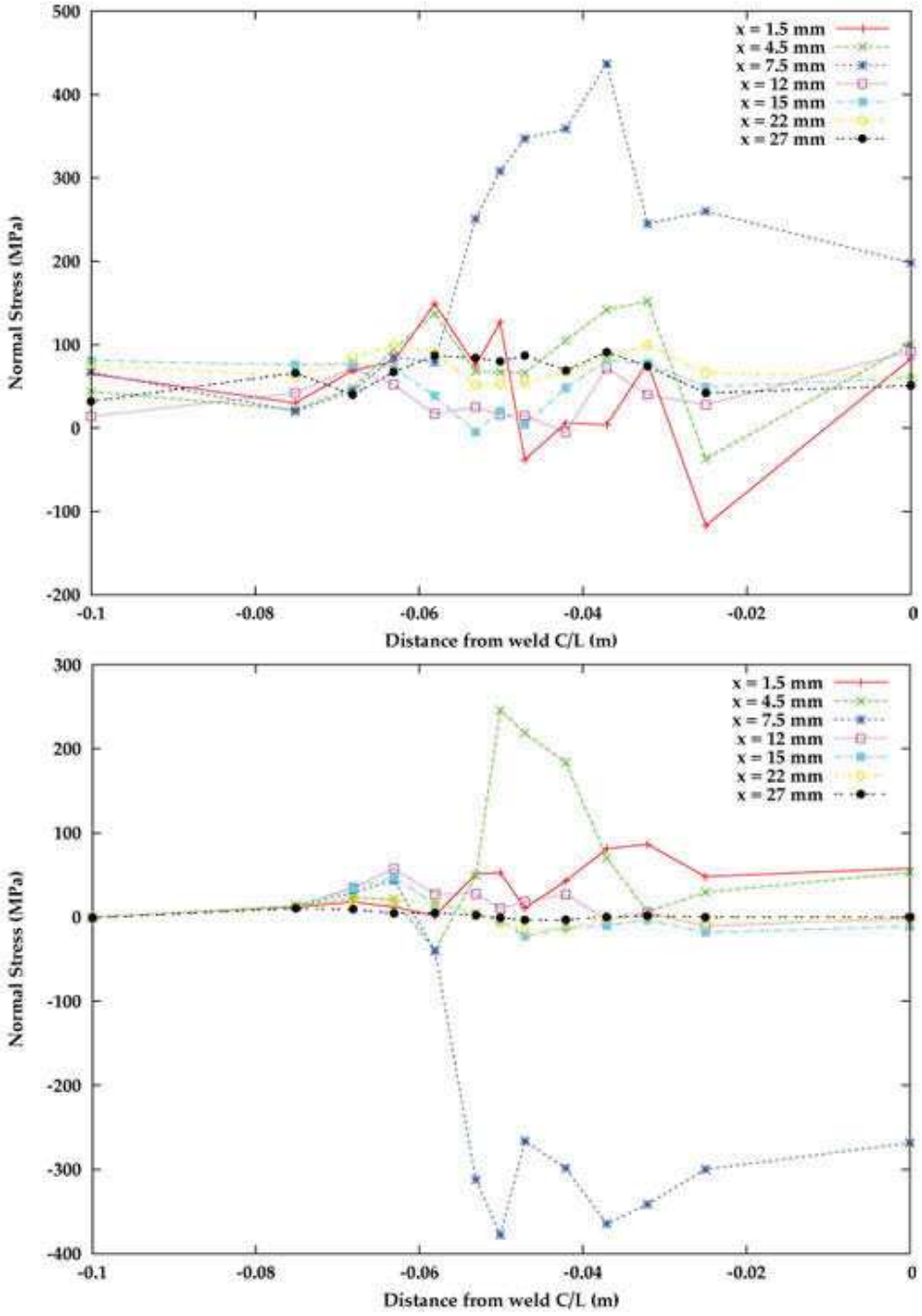

Figure 25: *Measured (top) and computed (bottom) normal residual stress in the small panel in the plane normal to the weld direction is shown.*

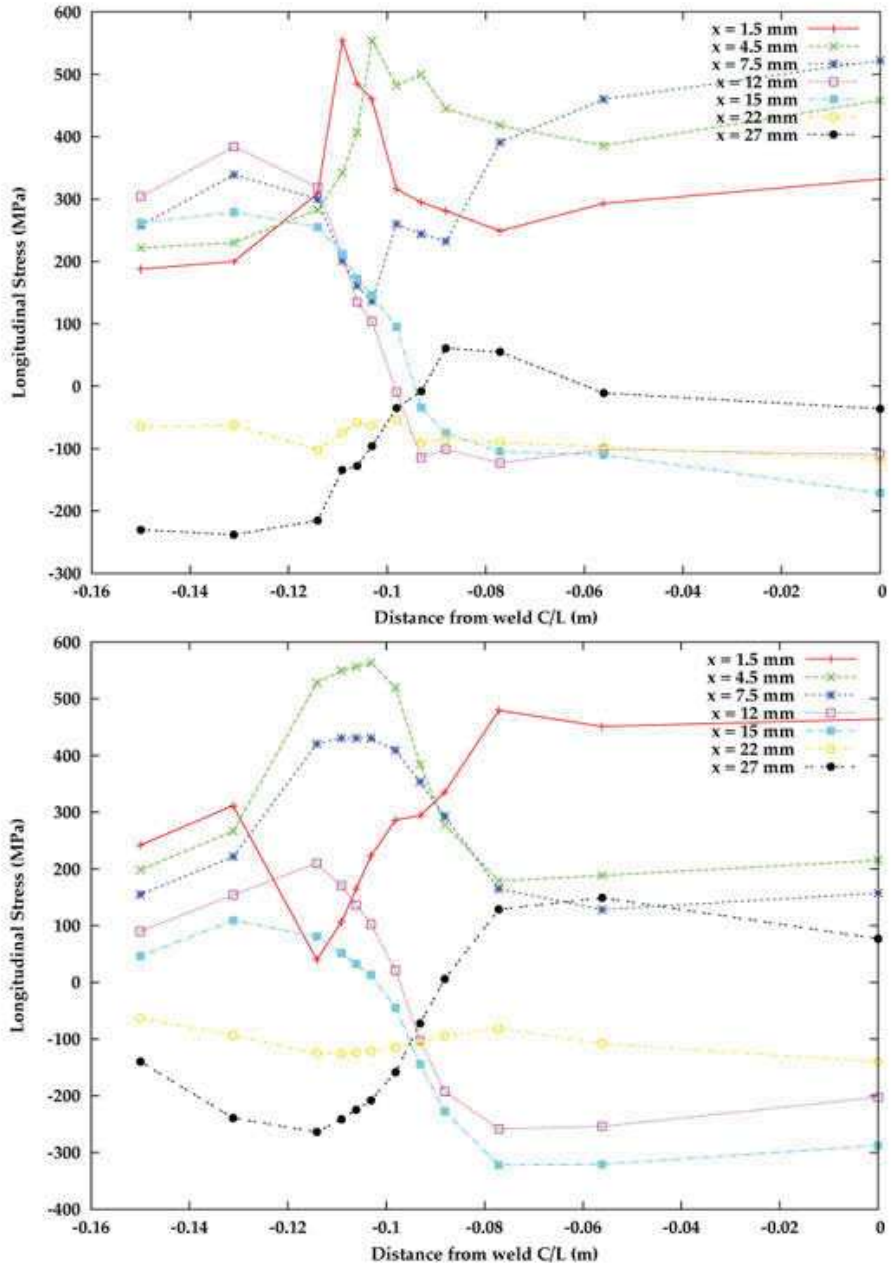

Figure 26: *Measured (top) and computed (bottom) longitudinal residual stress in the large panel in the plane parallel to the weld direction is shown.*

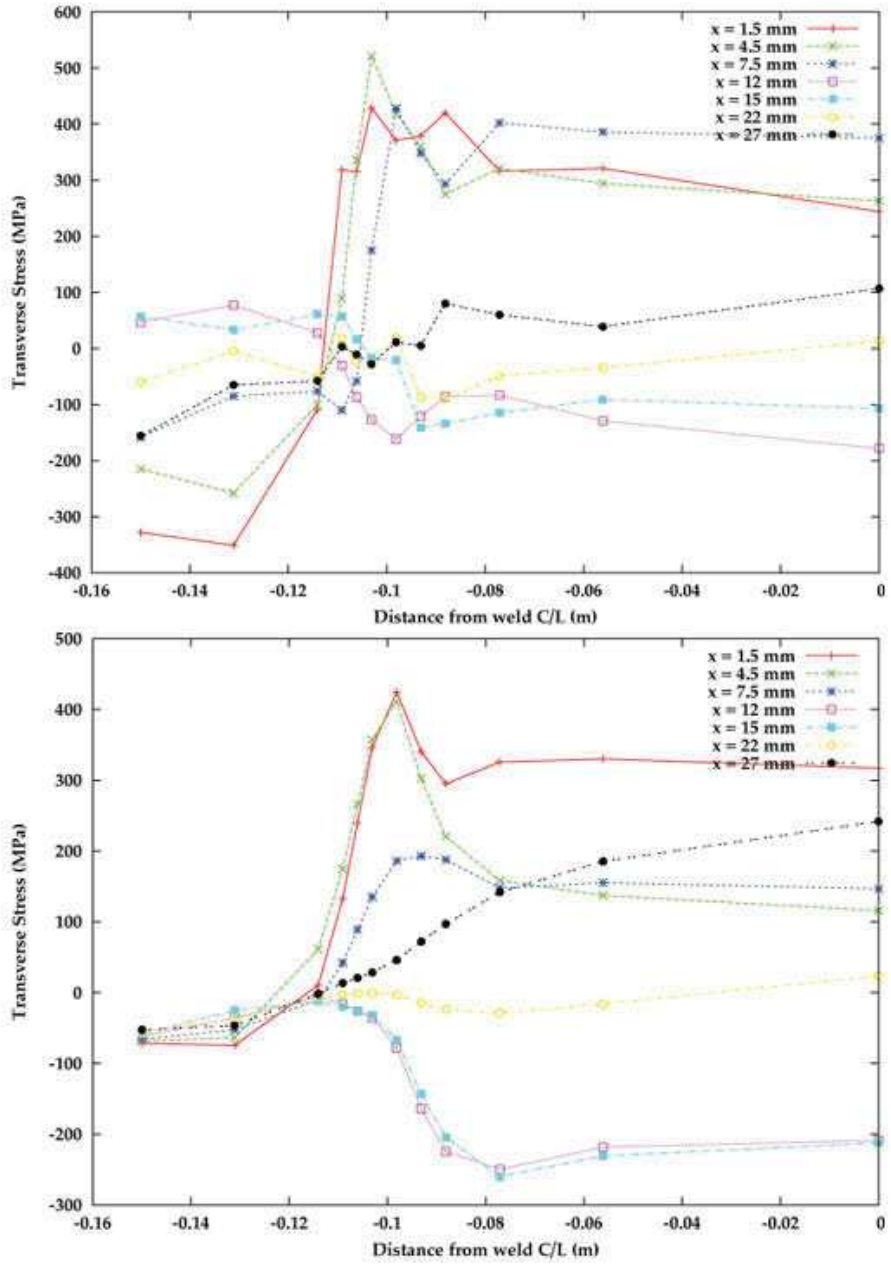

Figure 27: *Measured (top) and computed (bottom) transverse residual stress in the large panel in the plane parallel to the weld direction is shown.*

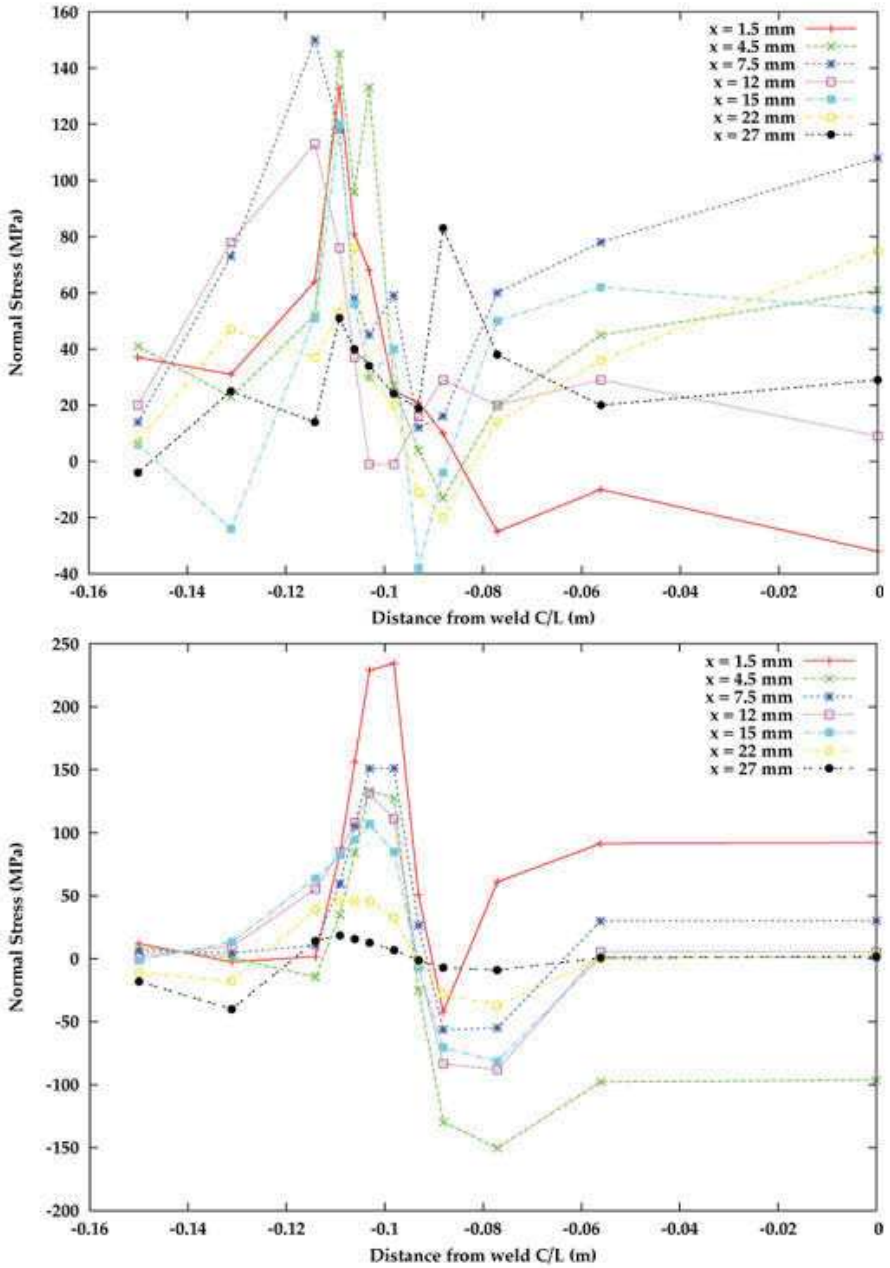

Figure 28: *Measured (top) and computed (bottom) normal residual stress in the large panel in the plane parallel to the weld direction is shown.*

5 Discussion of Comparison of Measured and Computed Residual Stress

The validation of the code for a computer model requires comparing computed results with experimental results. However, no rules have been established that define the best methods for measuring the difference between measured and computed results. The situation is particularly challenging for 3D continuum fields such as the field for the residual stress tensor. Sensors sample a finite number of points and each point integrates over a finite volume of space. The computer model must discretize space and time. From the sensor data points and the computer model data, one would like to compute 3D residual stress fields and evaluate the 'distance' between the measured and computed data fields. In mathematics the notion of distance between two functions or fields requires a norm. There is little or no agreement in the published literature on which norm or norms are best. It is the responsibility of the decision maker to decide if the agreement between the measured data and data computed by the model is sufficient to justify use of the model for a particular application [6] [9].

The numerical methodology for comparing measured and computed values of a 3D continuum field such as a stress tensor is a relatively immature. Figure 27 shows curves for computed and measured transverse stress. A person looking at the curves, might say the agreement is quite good. Figure 28 shows the difference between measured and computed transverse stresses that are plotted in Figure 27. The maximum differences range from -250MPa to 270 MPa while the stresses in Figure 27 range from -350 to +400 MPa.

For this project, the values of the computed residual stress data were mapped to the data points at which the residual stress was measured. Then two types of images were made. One image type is a jpg of the stress field determined by linear interpolation on the grid defined by the measured data points. The second image type is a plot of curves of the computed residual stress data and the residual stress along lines in the plane of the panel. For both types, one image of measured and one image of computed data is shown on each page to facilitate comparison. The residual stress measured at points on a coarse grid has a number of uncertainties associated with the neutron diffraction technique, the welding procedure and the manufacture of the plate. The computed values of the residual stress also have a number of uncertainties associated with the analysis. In the author's opinion, the greatest uncertainties in the computed values of the residual stress are associated with the material properties that are functions of temperature, microstructure and time. There is also a significant discretization error caused by using a finite mesh.

If the measured longitudinal, transverse and normal residual stresses are assumed to be principal stresses and the associated Cartesian directions are assumed to be the associated eigenvectors, then the measured values define the field of the stress tensor. The computed residual stress does not assume that the longitudinal, transverse and normal residual

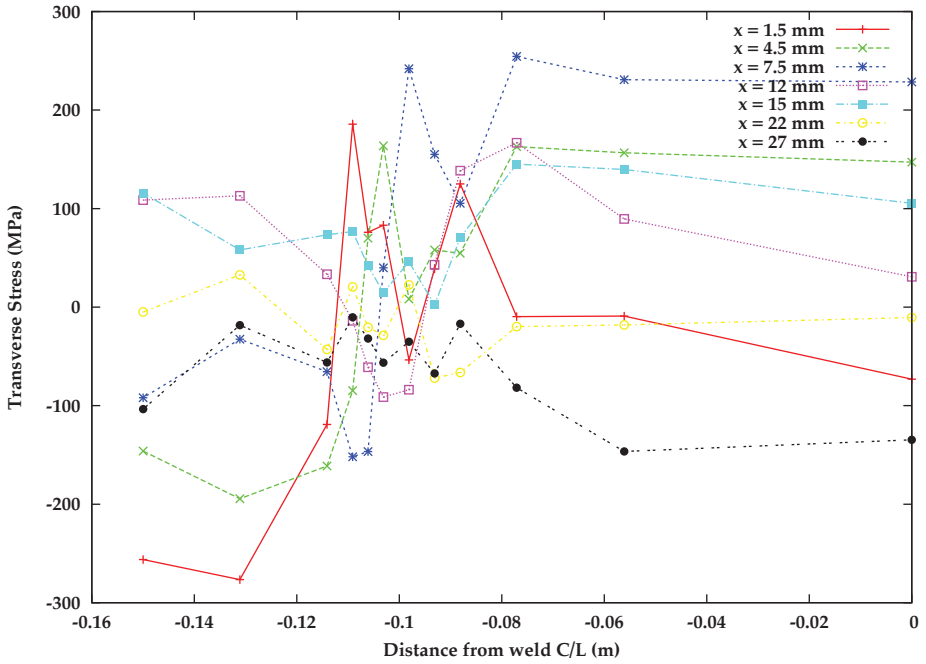

Figure 29: *The difference between the computed and measured transverse residual stress in the large panel in the plane parallel to the weld direction is shown. Compare to Fig. 27.*

stresses are principal stresses. See [2] for images of the computed principal stresses. It would be possible to compute the deviation of the computed principal stresses from the Cartesian axes and thus assess the error in assuming the Cartesian directions are directions of principal stresses.

The computed stresses are kinematically admissible stresses, i.e., the displacement field is C^0 continuous, satisfies Dirichlet or prescribed boundary conditions, the strain is a function of the symmetrized displacement gradient and the 4th order elasticity-plasticity tensor maps the strain tensor to the stress tensor. A statically admissible stress field would be C^0 continuous, satisfies Neumann or traction boundary conditions and the momentum equation. In particular, a statically admissible stress field is in equilibrium with zero traction boundary conditions. The Prager-Synge hyper-circle theorem states that the exact solution is bounded between the kinematically admissible and the statically admissible solutions. See Mashie [7] for further details.

6 Recommendations and Future Work

Based on past and current experience, the following recommendation and future work are suggested:

A virtual Design of Experiment (DOE) should be done to determine the sensitivity of the solution to model parameters. This would enable the agreement between measured and computed residual stress to be improved. The computed longitudinal stresses in the weld metal appear to be higher than the measured longitudinal stresses. This higher tensile residual stress in the weld metal could generate the higher longitudinal compressive stress just below the high tensile stress. This suggests that it would be worth doing a DOE analysis to compute the sensitivity to changes in the yield stress of martensite and bainite phases to determine if this improves the agreement between measured and computed residual stress.

The effect of martensite on the tempering to reduce the hardness of martensite formed in one weld pass by a later pass should be analyzed. This reduction in hardness suggests that the yield stress of martensite be reduced from approximately 900 MPa of the untempered martensite. If a model is developed for tempering of martensite, then the model could be included in the computer model.

Hardness measurements of the plate suggest that the hardness has a significant fluctuations in space, i.e., it is not homogeneous. It would be of interest to study the effect of such fluctuations on the residual stress. Transformation plasticity is a result of fluctuations at the micro-scale. However, the author is not aware of investigations of the effects of fluctuations at the macro-scale level.

The meshing could be further improved, particularly the stopping points of each weld pass. Goldak Technologies Inc. is exploring ways to do this, such as domain decomposition with a small domain with a fine mesh and space-time FEM analysis with a graded mesh.

References

[1] S. Tiku, N. Pussegoda, D. Begg, Monitoring of Welding Induced Strains during Cladding, DRDC Atlantic CR 2008-114, 2008.

[2] J. Goldak, Thermo-mechanical modelling of welding induced strains: Numerical validation of the weld build-up process, DRDC Atlantic CR 2008-283, 2008.

[3] J. Goldak, M.Akhlaghi, Computational Welding Mechanics, Springer, ISBN 0-387-23287-7 (2005).

[4] J. Goldak, J. Zhou, S. Tchernov, D. Downey, S. Wang, B. He, Predicting Distortion and Residual Stress in Complex Welded Structures by Designers, 7th International Trends in Welding Research, Callaway Gardens Resort, Pine Mountain, Georgia, USA, (2005) 531.

[5] J. A. Goldak, A. Chakravarti and M. J. Bibby, A New Finite Element Model for Welding Heat Sources, Trans. AIME., Vol. 15B, (1984) 299.

[6] Guide for Verification and Validation in Computational Solid Mechanics, ASME V&V 10-2006

[7] Akbar Mashaie, Error Estimates for Finite-Element Solutions of Elliptic Boundary Value Problems, Ph.D. thesis, Carleton University, 1990.

[8] S. McLaughlin, C.J. Bayley, Residual Stress Characterization of Weld Built-Up Panels; A Neutron Diffraction Study, DRDC Atlantic TM 2009-264, 2010

[9] D. Radaj and L-E Lindgren, Verification and Validation in Computational Weld Mechanics, in Mathematical Modeling of Weld Phenomena 8, H. Cerjak, H. K. D. H. Bhadeshia, E. Kozenchnik, (2006) 1039-1051.

Distribution list

DRDC Atlantic CR 2009-222

Internal distribution

2 DRDC Atlantic DLP Attn Christopher Bayley (1 Hardcopy)

1 DRDC Atlantic DLA SUBSLA Scientific Advisor (Attn: J. Porter)

1 DRDC Atlantic SH/WP Attn: N. Pegg (1 Hardcopy)

3 Library (1 Hardcopy, 2 CDs)

Total internal copies: 7

External distribution

1 DRDKIM

1 Library and Archives Canada

1 Goldak Technologies Inc. (Attn Dr. J. Goldak)
3745 Revelstoke Drive
Ottawa ON K1V7C2

1 DMEPM(SM-4-2)
LSTL, 555 blvd de la Carriere, 5-WB06
NDHQ - 101 Colonel By Dr
Ottawa ON K1A 0K2

1 DMSS 2-4-3 Materials and Welding Engineer: (Attn Dr. J. Huang)
LSTL, 555 blvd de la Carriere, 5-WB06
NDHQ - 101 Colonel By Dr
Ottawa ON K1A 0K2

Total external copies: 5

Total copies: 12

Attn: Military Archivist, Government Records Branch

This page intentionally left blank.

DOCUMENT CONTROL DATA

(Security classification of title, body of abstract and indexing annotation must be entered when document is classified)

1. ORIGINATOR (the name and address of the organization preparing the document. Organizations for whom the document was prepared, e.g. Centre sponsoring a contractor's report, or tasking agency, are entered in section 8.)

   Goldak Technology Inc.
   3745 Revelstoke Drive, Ottawa, ON, K1V7C2, Canada

2. SECURITY CLASSIFICATION (overall security classification of the document including special warning terms if applicable).

   UNCLASSIFIED

3. TITLE (the complete document title as indicated on the title page. Its classification should be indicated by the appropriate abbreviation (S,C,R or U) in parentheses after the title).

   Validations of Computational Weld Models: Comparison of Residual Stresses

4. AUTHORS (last name, first name, middle initial)

   John Goldak,

5. DATE OF PUBLICATION (month and year of publication of document)	6a. NO. OF PAGES (total containing information. Include Annexes, Appendices, etc).	6b. NO. OF REFS (total cited in document)
August 2010	52	9

7. DESCRIPTIVE NOTES (the category of the document, e.g. technical report, technical note or memorandum. If appropriate, enter the type of report, e.g. interim, progress, summary, annual or final. Give the inclusive dates when a specific reporting period is covered).

   Contract Report

8. SPONSORING ACTIVITY (the name of the department project office or laboratory sponsoring the research and development. Include address).

   Defence R&D Canada – Atlantic
   P.O. Box 1012, Dartmouth, Nova Scotia, Canada B2Y 3Z7

9a. PROJECT NO. (the applicable research and development project number under which the document was written. Specify whether project).	9b. GRANT OR CONTRACT NO. (if appropriate, the applicable number under which the document was written).
11ga08-04	W7707-098193

10a. ORIGINATOR'S DOCUMENT NUMBER (the official document number by which the document is identified by the originating activity. This number must be unique.)	10b. OTHER DOCUMENT NOs. (Any other numbers which may be assigned this document either by the originator or by the sponsor.)
DRDC Atlantic CR 2009-222	

11. DOCUMENT AVAILABILITY (any limitations on further dissemination of the document, other than those imposed by security classification)

   (X) Unlimited distribution
   ( ) Defence departments and defence contractors; further distribution only as approved
   ( ) Defence departments and Canadian defence contractors; further distribution only as approved
   ( ) Government departments and agencies; further distribution only as approved
   ( ) Defence departments; further distribution only as approved
   ( ) Other (please specify):

12. DOCUMENT ANNOUNCEMENT (any limitation to the bibliographic announcement of this document. This will normally correspond to the Document Availability (11). However, where further distribution beyond the audience specified in (11) is possible, a wider announcement audience may be selected).

13. ABSTRACT (a brief and factual summary of the document. It may also appear elsewhere in the body of the document itself. It is highly desirable that the abstract of classified documents be unclassified. Each paragraph of the abstract shall begin with an indication of the security classification of the information in the paragraph (unless the document itself is unclassified) represented as (S), (C), (R), or (U). It is not necessary to include here abstracts in both official languages unless the text is bilingual).

The objective of this project was to validate the capability of *VrWeld* to simulate the weld build-up process in two experimental setups. Setup I had a central depression with dimensions of $100 \times 100 \times 3$ mm, while Setup II had a central depression with dimensions of $200 \times 200 \times 3$ mm.

This report documents the validation of the computer model's capability to compute residual stress in overlay weld repairs of this type, i.e., does the model predict the measured residual stress with sufficient accuracy, reliability and robustness.

For this project, the values of the computed residual stress data were mapped to the data points at which the residual stress was measured. Then two types of plots were made. The first is an image of the stress field determined by linear interpolation onto the prefered grid. The second is a plot of curves of the computed residual stress data and the residual stress along lines in the plane of the panel. For both types, one image of measured and one image of computed data is shown on each page to facilitate comparison.

Whether the model predicts the measured residual stress with sufficient accuracy, reliability and robustness for a particular analysis would depend on the analysis.

14. KEYWORDS, DESCRIPTORS or IDENTIFIERS (technically meaningful terms or short phrases that characterize a document and could be helpful in cataloguing the document. They should be selected so that no security classification is required. Identifiers, such as equipment model designation, trade name, military project code name, geographic location may also be included. If possible keywords should be selected from a published thesaurus. e.g. Thesaurus of Engineering and Scientific Terms (TEST) and that thesaurus-identified. If it not possible to select indexing terms which are Unclassified, the classification of each should be indicated as with the title).

Thermo-mechanical model, FEM, Submarine Service Level Agreement, HY-80, Weld Build-up, Weld Cladding, Residual strain, Welding Distortion, Neutron Diffraction

This page intentionally left blank.

Defence R&D Canada

Canada's leader in defence
and National Security
Science and Technology

R & D pour la défense Canada

Chef de file au Canada en matière
de science et de technologie pour
la défense et la sécurité nationale

DEFENCE **DÉFENSE**

www.drdc-rddc.gc.ca